Journal of Science and Technology in Civil Engineering, NUCE 2021. 15 (3): 109–122

AN EFFECTIVE HIGH-ORDER ELEMENT FOR ANALYSIS OF TWO-DIMENSIONAL LINEAR PROBLEM USING SBFEM

Nguyen Van Chung[a,*], Nguyen Thanh Him[a], Bui Quoc Khiem[b], Pham Ngoc Tien[b]

[a]*Faculty of Civil Engineering, HCMC University of Technology and Education, 01 Vo Van Ngan street, Thu Duc City, Ho Chi Minh City, Vietnam*
[b]*Faculty of Civil Engineering, Mientrung University of Civil Engineering, 24 Nguyen Du street, Ward 7, Tuy Hoa City, Phu Yen Province, Vietnam*

Article history:
Received 10/12/2020, Revised 16/06/2021, Accepted 18/06/2021

Abstract

The scaled boundary finite element method (SBFEM) is a semi-analytical method, whose versatility, accuracy, and efficiency are not only equal to, but potentially better than the finite element method and the boundary element method for certain problems. This paper investigates the possibility of using an efficient high-order polynomial element in the SBFEM to form the approximation in the circumferential direction. The governing equations are formulated from the classical linear elasticity theory via the SBFEM technique. The scaled boundary finite element equations are formulated within a general framework integrating the influence of the distributed body source, mixed boundary conditions, contributions the side face with either prescribed surface load or prescribed displacement. The position of scaling center is considered for modeling problem. The proposed method is evaluated by solving two-dimensional linear problem. A selected set of results is reported to demonstrate the accuracy and convergence of the proposed method for solving problems in general boundary conditions.

Keywords: SBFEM; high-order element; scaling center; linear problem.

https://doi.org/10.31814/stce.nuce2021-15(3)-09

1. Introduction

The scaled boundary finite element method (SBFEM) has been found an attractive alternative analysis tool in the solving complicated engineering problems, unbounded domains, variation of material properties and loading [1–6]. Recently, several engineering problems have been efficiently solved and accurately investigated by exploring the SBFEM including piezoelectric materials [7], electrostatic problem [8], concentrated load on elastic medium [9], circular defining curve for geomechanics applications [10] and many engineering problems (e.g., [11–20]. Basing on published studies that have demonstrated the significant progress of the SBFEM in the analysis of numerous engineering problems.

The smooth solutions within the body of the scaled boundary finite element method are obtained analytically in the radial direction, while numerical solutions are obtained in the circumferential direction by the finite element standard with boundary discretization and shape functions. When the finite

*Corresponding author. *E-mail address:* chungnv@hcmute.edu.vn (Chung, N. V.)

element method is applied for continuum problems, use of element higher than quadratic is seldom economical. However, this argument does not apply to the scaled boundary finite element method. Firstly, the elements are reduced one dimension for comparison with the finite elements to solve the same problem. Secondly, the domain stiffness matrix is always populated in the scaled boundary finite element method. Most previous work using the scaled boundary finite element method has employed in a problem-dependent style. Vu and Deeks [3] were developed the hierarchical approach and used higher-order shape functions to analysis plain strain problem under single boundary conditions. Recently, Chung [10] have investigated to use the exact description of circular defining cure to analyze geo-mechanics in unbounded domain. The published research showed that the solution procedure can be reduced the solution error and the good accuracy. The main factors such as accurate results of the method will be affected such as types of boundary value problems, kind of shape functions for approximation, domain geometry, solving eigenvalue problems will be affected to the accurate solutions of the method. This paper investigates the possibility of using higher-order polynomial functions to describe shape functions in the scaled boundary finite element method for solving two-dimensional linear problem in general boundary conditions.

The paper is outlined as follows. The governing equations for two-dimensional linear problem are given in governing equations part. The scaled boundary finite element equations are summarized in scaled doundary formulation part. High-order shape functions illustrates the different types of polynomial shape functions in the scaled boundary finite element method. Some concluding remarks are depicted in performance application.

2. Governing Equations

Base on the classical theory of linear elasticity, equilibrium equations, stress-strain relationship, and strain-displacement for a two dimensional-linear problem can be expressed by

$$\mathbf{L}^T\boldsymbol{\sigma} + \mathbf{b} = \mathbf{0} \tag{1}$$

$$\boldsymbol{\sigma} = \mathbf{D}\bar{\boldsymbol{\varepsilon}} \tag{2}$$

$$\bar{\boldsymbol{\varepsilon}} = \mathbf{L}\mathbf{u} \tag{3}$$

where $\mathbf{u}(\mathbf{x}), \bar{\boldsymbol{\varepsilon}}(\mathbf{x}), \boldsymbol{\sigma}(\mathbf{x}), \mathbf{b}, \mathbf{D}$ and $\mathbf{L}$ denoting, respectively, a vector containing displacement components, a vector containing strain components, a vector containing stress components, a vector containing body components, a modulus matrix involving material constants, and a two-dimensional, linear differential operator defined, by

$$\mathbf{L} = \mathbf{L}_1\frac{\partial}{\partial x_1} + \mathbf{L}_2\frac{\partial}{\partial x_2}; \quad \mathbf{L}_1 = \begin{bmatrix} 1 & 0 \\ 0 & 0 \\ 0 & 1 \end{bmatrix}; \quad \mathbf{L}_2 = \begin{bmatrix} 0 & 0 \\ 0 & 1 \\ 1 & 0 \end{bmatrix} \tag{4}$$

The traction $\mathbf{t}(\mathbf{x})$ can be related to the body force $\boldsymbol{\sigma}(\mathbf{x})$ and the outward unit normal vector $n(\mathbf{x})$ by

$$\mathbf{t} = \begin{bmatrix} n_1\mathbf{I} & n_2\mathbf{I} \end{bmatrix}\boldsymbol{\sigma} \tag{5}$$

where n_1 and n_2 are components of $n(\mathbf{x})$.

By applying the standard weighted residual technique to the law of conservation (1), then integrating certain integral by parts via Gauss-divergence theorem, and finally employing the relations (2) and (3), the weak-form equation in terms of the state variable is given by

$$\int_{\Omega} (\mathbf{Lw})^T \mathbf{D}(\mathbf{Lu}) dA = \int_{\partial\Omega} \mathbf{w}^T \mathbf{t} dl + \int_{\Omega} \mathbf{w}^T \mathbf{b} dA \tag{6}$$

where $\mathbf{w}$ is a component vector of test functions satisfying the integrability condition.

$$\int_{\Omega} \left[(\mathbf{Lw})^T (\mathbf{Lw}) + \mathbf{w}^T \mathbf{w} \right] dA < \infty \tag{7}$$

3. Scaled Boundary Formulation

3.1. Formulation

Let introduce the scaled boundary finite element approximation of the displacement field $\mathbf{u}$ and the weight function $\mathbf{w}$ can be approximated by

$$\mathbf{u}^h = \mathbf{u}^h(\xi, s) = \mathbf{N}^S \mathbf{U}^h; \quad \mathbf{w}^h = \mathbf{w}^h(\xi, s) = \mathbf{N}^S \mathbf{W}^h \tag{8}$$

where $\mathbf{N}^S$ is a matrix containing all basis functions used for approximating the solution, $\mathbf{U}^h$ is a vector containing all unknown nodal functions, and $\mathbf{W}^h$ is a vector containing all arbitrary nodal functions.

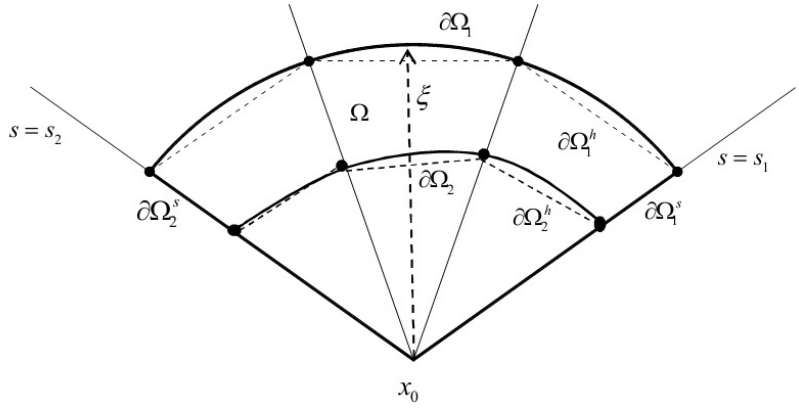

Figure 1. Schematic of a generic body Ω and its approximation Ω^h

By applying the above approximations to the weak-form equation (6) for a generic two-dimensional in the $\xi - s$ plane and the approximate body is denoted Ω^h as shown in Fig. 1. In particular, the approximate outer boundary $\partial\Omega_1^h$, the approximate inner boundary $\partial\Omega_2^h$, the side-face-1 $\partial\Omega_1^s$ and the side-face-2 $\partial\Omega_2^s$ are full described by $\xi_1 \leq \xi \leq \xi_2$, $s_1 \leq s \leq s_2$. Then performing the integration by parts of certain integral via Gauss-divergence theorem, and finally exploiting arbitrariness of $\mathbf{W}^h$, it leads to the scaled boundary finite element equations:

$$\xi^2 \mathbf{E}_0 \mathbf{U}^h_{,\xi\xi} + \xi(\mathbf{E}_0 + \mathbf{E}_1^T - \mathbf{E}_1)\mathbf{U}^h_{,\xi} - \mathbf{E}_2 \mathbf{U}^h + \xi \mathbf{F}^t + \xi^2 \mathbf{F}^b = \mathbf{0}, \quad \forall \xi \in (\xi_1, \xi_2) \tag{9}$$

$$\mathbf{Q}^h(\xi_1) = -\mathbf{P}_1 \tag{10}$$

$$\mathbf{Q}^h(\xi_2) = \mathbf{P}_2 \tag{11}$$

where $\mathbf{Q}^h(\xi) = \xi \mathbf{E}_0 \mathbf{U}^h_{,\xi} + \mathbf{E}_1^T \mathbf{U}^h$ and all involved matrices are given by

$$\mathbf{E}_0 = \int_{s_1}^{s_2} \mathbf{B}_1^T \mathbf{D} \mathbf{B}_1 J ds; \quad \mathbf{E}_1 = \int_{s_1}^{s_2} \mathbf{B}_2^T \mathbf{D} \mathbf{B}_1 J ds; \quad \mathbf{E}_2 = \int_{s_1}^{s_2} \mathbf{B}_2^T \mathbf{D} \mathbf{B}_2 J ds \tag{12}$$

$$\mathbf{P}_1 = \int_{s_i}^{s_o} (\mathbf{N}^S)^T \mathbf{t}_1 \xi_1 J^s ds; \quad \mathbf{P}_2 = \int_{s_i}^{s_o} (\mathbf{N}^S)^T \mathbf{t}_2 \xi_2 J^s(s) ds; \quad J^s = \sqrt{(d\hat{x}_1/ds)^2 + (d\hat{x}_2/ds)^2} \tag{13}$$

$$\mathbf{F}^b = \int_{s_1}^{s_2} (\mathbf{N}^S)^T \mathbf{b} J ds; \quad \mathbf{F}^t = \mathbf{F}_1^t + \mathbf{F}_2^t; \quad \mathbf{F}_1^t = (\mathbf{N}_1^S)^T \mathbf{t}_1^s J_1^\xi; \quad \mathbf{F}_2^t = (\mathbf{N}_2^S)^T \mathbf{t}_2^s J_2^\xi \tag{14}$$

with $\mathbf{B}_1 = \mathbf{b}_1^h \mathbf{N}^S$, $\mathbf{B}_2 = \mathbf{b}_2^h \mathbf{B}^S$, $\mathbf{B}^S = d\mathbf{N}^S/ds$, $\mathbf{t}_1$, $\mathbf{t}_2$, $\mathbf{t}_1^s$, $\mathbf{t}_2^s$ denoting the surface fluxes on the boundaries $\partial\Omega_1$, $\partial\Omega_2$, $\partial\Omega_1^s$, $\partial\Omega_2^s$ shown in Fig. 1, $J_1^\xi = J_\xi(s_1)$, $J_2^\xi = J_\xi(s_2)$, and $J^\xi(s) = \sqrt{\hat{x}_1^2 + \hat{x}_2^2}$. The vector $\mathbf{U}^h$ is first partitioned and rearranged into known and unknown parts as $\mathbf{U}^h = \{\mathbf{U}^{hu} \quad \mathbf{U}^{hc}\}^T$ where $\mathbf{U}^{hu}$ contains only unknown functions and $\mathbf{U}^{hc}$ contains the remaining known functions associated with the prescribed state variable on the side face. Consistent with the partition of the vector $\mathbf{U}^h$, the vectors $\mathbf{F}^t$, $\mathbf{F}^b$, $\mathbf{P}_1$, $\mathbf{P}_2$ and $\mathbf{Q}^h$ can also be partitioned into $\mathbf{F}^t = \{\mathbf{F}^{tu} \quad \mathbf{F}^{tc}\}^T$,$\mathbf{F}^t = \{\mathbf{F}^{tu} \quad \mathbf{F}^{tc}\}^T$, $\mathbf{P}_1 = \{\mathbf{P}_1^u \quad \mathbf{P}_1^c\}^T$, $\mathbf{P}_2 = \{\mathbf{P}_2^u \quad \mathbf{P}_2^c\}^T$ and $\mathbf{Q}^h = \{\mathbf{Q}^{hu} \quad \mathbf{Q}^{hc}\}^T$. From this partition, the original system (9) can be reduced to [10]

$$\xi^2 \mathbf{E}_0^{uu} \mathbf{U}^{hu}_{,\xi\xi} + \xi \left[\mathbf{E}_0^{uu} + (\mathbf{E}_1^{uu})^T - \mathbf{E}_1^{uu}\right] \mathbf{U}^{hu}_{,\xi} - \mathbf{E}_2^{uu} \mathbf{U}^{hu} = -\xi \mathbf{F}^{tu} - \xi^2 \mathbf{F}^{bu} - \mathbf{F}^{suu} \forall \xi \in (\xi_1, \xi_2) \tag{15}$$

$$\mathbf{Q}^{hu}(\xi_1) = -\mathbf{P}_1^u \tag{16}$$

$$\mathbf{Q}^{hu}(\xi_2) = \mathbf{P}_2^u \tag{17}$$

where $\mathbf{U}^{hu}_{,\xi}$, $\mathbf{U}^{hu}_{,\xi\xi}$ the first, the second derivative of unknown function; $\mathbf{F}^{suu}$ is the known vector obtained from the prescribed state variable on the side face and $\mathbf{E}_0^{uu}$, $\mathbf{E}_1^{uu}$ and $\mathbf{E}_2^{uu}$ result directly from the partition.

3.2. Solution methodology

The general solution can be separated in two parts, a homogenous solution, and a particular solution. The homogenous solution of a system of linear, second order, differential equations is determined by solving the eigenvalue problem resulting adopting the standard theory of differential equations with constant coefficients. In contract, the particular solution is determined by adopting the technique of undetermined coefficients which depends on the form of applied traction on free surface. Firstly, a homogeneous solution of the system of linear, second-order, Euler-Cauchy differential equations (15), denoted by $\mathbf{U}_0^{hu}$, can readily be obtained in a form

$$\mathbf{U}_0^{hu}(\xi) = \sum_{i=1}^{2m\Lambda} c_i \xi^{\lambda_i} \boldsymbol{\psi}_i^u \tag{18}$$

where m is the number of unknown functions contained in $\mathbf{U}_0^{hu}$, λ_i is termed the modal scaling factor, $\boldsymbol{\psi}_i^u$ is a vector representing the i^{th} mode of the state variable, and c_i are arbitrary constants denoting the contribution of each mode to the solution. The nodal scaling factor λ_i and the corresponding $\boldsymbol{\psi}_i^u$ can be obtained by solving a system of linear algebraic equations

$$\mathbf{A}\mathbf{X}_i = \lambda_i \mathbf{X}_i \tag{19}$$

where $\mathbf{X}_i = \left\{\boldsymbol{\psi}_i^u \;\; \mathbf{q}_i^u\right\}^T$, $\mathbf{q}_i^u = \left\{\lambda_i \mathbf{E}_0^{uu} + \left(\mathbf{E}_1^{uu}\right)^T\right\}\boldsymbol{\psi}_i^u$, and the matrix $\mathbf{A}$ is given by

$$\mathbf{A} = \begin{bmatrix} -(\mathbf{E}_0^{uu})^{-1}(\mathbf{E}_1^{uu})^T & (\mathbf{E}_0^{uu})^{-1} \\ \mathbf{E}_2^{uu} - \mathbf{E}_1^{uu}(\mathbf{E}_0^{uu})^{-1}(\mathbf{E}_1^{uu})^T & \mathbf{E}_1^{uu}(\mathbf{E}_0^{uu})^{-1} \end{bmatrix} \tag{20}$$

All eigen-pairs $\{\lambda_i, \mathbf{X}_i\}$ can be obtained by a selected efficient numerical technique. Let $\boldsymbol{\lambda}^+$ and $\boldsymbol{\lambda}^-$ be diagonal matrices containing eigenvalues with the positive and negative real parts, respectively. Also, let $\boldsymbol{\Phi}^{\psi+}$ and $\boldsymbol{\Phi}^{q+}$ be matrices whose columns containing, respectively, all vectors $\boldsymbol{\psi}_i^u$ and $\boldsymbol{q}_i^u$ obtained from the eigenvectors $\mathbf{X}_i = \left\{\boldsymbol{\psi}_i^u \;\; \mathbf{q}_i^u\right\}^T$ associated with all eigenvalues contained in $\boldsymbol{\lambda}^+$ and let $\boldsymbol{\Phi}^{\psi-}$ and $\boldsymbol{\Phi}^{q-}$ be matrices whose columns containing, respectively, all vectors $\boldsymbol{\psi}_i^u$ and $\mathbf{q}_i^u$ obtained from the eigenvectors $\mathbf{X}_i = \left\{\boldsymbol{\psi}_i^u \;\; \mathbf{q}_i^u\right\}^T$ associated with all eigenvalues contained in $\boldsymbol{\lambda}^-$. Now, the homogeneous solutions $\mathbf{U}_0^{hu}$ and $\mathbf{Q}_0^{hu}$ are given by

$$\mathbf{U}_0^{hu}(\xi) = \boldsymbol{\Phi}^{\psi+}\boldsymbol{\Pi}^+(\xi)\mathbf{C}^+ + \boldsymbol{\Phi}^{\psi-}\boldsymbol{\Pi}^-(\xi)\mathbf{C}^-; \quad \mathbf{Q}_0^{hu}(\xi) = \boldsymbol{\Phi}^{q+}\boldsymbol{\Pi}^+(\xi)\mathbf{C}^+ + \boldsymbol{\Phi}^{q-}\boldsymbol{\Pi}^-(\xi)\mathbf{C}^- \tag{21}$$

where $\boldsymbol{\Pi}^+$ and $\boldsymbol{\Pi}^-$are diagonal matrices obtained by replacing the diagonal entries λ_i of the matrices $\boldsymbol{\lambda}^+$ and $\boldsymbol{\lambda}^-$ by the a function ξ^{λ_i}, respectively; and $\mathbf{C}^+$ and $\mathbf{C}^-$ are vectors containing arbitrary constants representing the contribution of each mode.

A particular solution of (15), denoted by $\mathbf{U}_1^{hu}$, associated with the distributed body source, the surface flux on the side face and the prescribed state variable on the side face can also be obtained from a standard procedure in the theory of differential equations such as the method of undetermined coefficient. Once the particular solution $\mathbf{U}_1^{hu}$ is obtained [10], the corresponding particular nodal internal flux $\mathbf{Q}_1^{hu}$ can be calculated. Finally, the general solution of (18) and the corresponding nodal internal flux are then given by

$$\mathbf{U}^{hu}(\xi) = \mathbf{U}_0^{hu}(\xi) + \mathbf{U}_1^{hu}(\xi) = \boldsymbol{\Phi}^{\psi+}\boldsymbol{\Pi}^+(\xi)\mathbf{C}^+ + \boldsymbol{\Phi}^{\psi-}\boldsymbol{\Pi}^-(\xi)\mathbf{C}^- + \mathbf{U}_1^{hu}(\xi) \tag{22}$$

$$\mathbf{Q}^{hu}(\xi) = \mathbf{Q}_0^{hu}(\xi) + \mathbf{Q}_1^{hu}(\xi) = \boldsymbol{\Phi}^{q+}\boldsymbol{\Pi}^+(\xi)\mathbf{C}^+ + \boldsymbol{\Phi}^{q-}\boldsymbol{\Pi}^-(\xi)\mathbf{C}^- + \mathbf{Q}_1^{hu}(\xi) \tag{23}$$

To determine the constants contained in $\mathbf{C}^+$ and $\mathbf{C}^-$, the boundary conditions on both inner and outer boundaries are enforced. By enforcing the conditions (16)–(17), it gives rise to

$$\begin{Bmatrix} \mathbf{C}^+ \\ \mathbf{C}^- \end{Bmatrix} = \begin{bmatrix} \boldsymbol{\Phi}^{q+}\boldsymbol{\Pi}^+(\xi_1) & \boldsymbol{\Phi}^{q-}\boldsymbol{\Pi}^-(\xi_1) \\ \boldsymbol{\Phi}^{q+}\boldsymbol{\Pi}^+(\xi_2) & \boldsymbol{\Phi}^{q-}\boldsymbol{\Pi}^-(\xi_2) \end{bmatrix}^{-1} \left(\begin{Bmatrix} -\mathbf{P}_1^u \\ \mathbf{P}_2^u \end{Bmatrix} - \begin{Bmatrix} \mathbf{Q}_1^{hu}(\xi_1) \\ \mathbf{Q}_1^{hu}(\xi_2) \end{Bmatrix} \right) \tag{24}$$

From (24), it can readily be obtained and substituting (22) into its yields

$$\mathbf{K}\begin{Bmatrix} \mathbf{U}^{hu}(\xi_1) \\ \mathbf{U}^{hu}(\xi_2) \end{Bmatrix} = \begin{Bmatrix} -\mathbf{P}_1^u \\ \mathbf{P}_2^u \end{Bmatrix} + \mathbf{K}\begin{Bmatrix} \mathbf{U}_1^{hu}(\xi_1) \\ \mathbf{U}_1^{hu}(\xi_2) \end{Bmatrix} - \begin{Bmatrix} \mathbf{Q}_1^{hu}(\xi_1) \\ \mathbf{Q}_1^{hu}(\xi_2) \end{Bmatrix} \tag{25}$$

where the coefficient matrix $\mathbf{K}$, commonly termed the stiffness matrix, is given by

$$\mathbf{K} = \begin{bmatrix} \mathbf{\Phi}^{q+}\mathbf{\Pi}^{+}(\xi_1) & \mathbf{\Phi}^{q-}\mathbf{\Pi}^{-}(\xi_1) \\ \mathbf{\Phi}^{q+}\mathbf{\Pi}^{+}(\xi_2) & \mathbf{\Phi}^{q-}\mathbf{\Pi}^{-}(\xi_2) \end{bmatrix} \begin{bmatrix} \mathbf{\Phi}^{\psi+}\mathbf{\Pi}^{+}(\xi_1) & \mathbf{\Phi}^{\psi-}\mathbf{\Pi}^{-}(\xi_1) \\ \mathbf{\Phi}^{\psi+}\mathbf{\Pi}^{+}(\xi_2) & \mathbf{\Phi}^{\psi-}\mathbf{\Pi}^{-}(\xi_2) \end{bmatrix}^{-1} \tag{26}$$

By applying the prescribed surface flux and the state variable on both inner and outer boundaries, a system of linear algebraic equations (15) is sufficient for determining all involved unknowns. Once the unknowns on both the inner and outer boundaries are solved, the approximate field quantities such as the state variable and the surface flux within the body can readily be post-processed.

3.3. Higher-Order Shape Functions

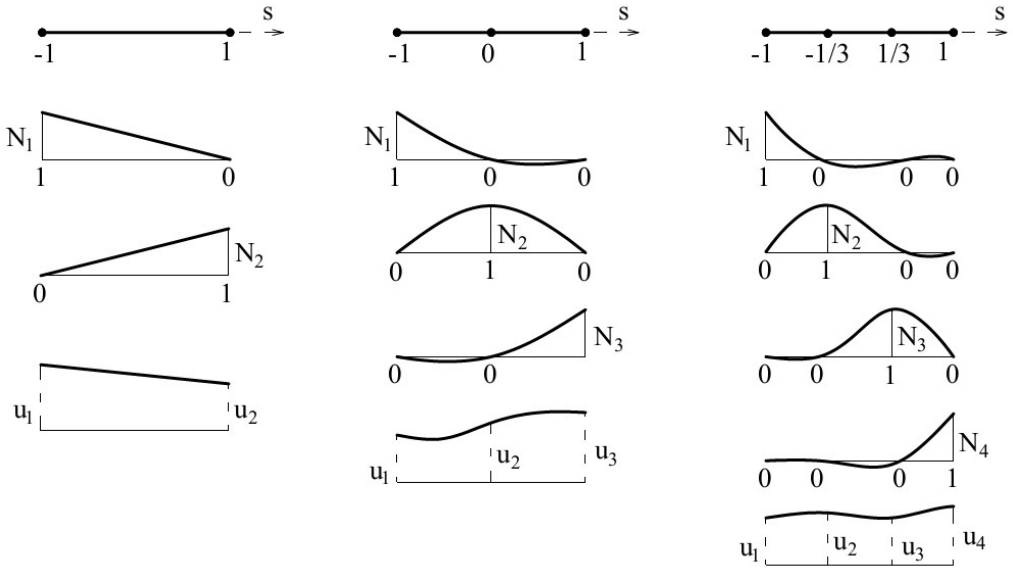

(a) 2-noded element (b) 3-noded element (c) 3-noded element

Figure 2. Shape functions

The scaled boundary finite element method has employed Lagrange shape functions with nodes equally spaced in the local element coordinate system. Shape functions are used to describe the domain geometry and to describe the solution in the boundary direction within each element. A shape function has unit value at the node and 0 at all other nodes in an element and shown in Fig. 2. Each element has ranging from -1 to $+1$ at local coordinates. For the 2-noded linear element, the shape functions are given explicitly as

$$\begin{aligned} N_1(s) &= \frac{1}{2}(1-s) \\ N_2(s) &= \frac{1}{2}(1+s) \end{aligned} \tag{27}$$

For the 3-noded quadratics element, the shape functions can be expressed simply as

$$\begin{aligned} N_1(s) &= -\frac{1}{2}s(1-s) \\ N_2(s) &= (1+s)(1-s) \\ N_3(s) &= \frac{1}{2}s(1+s) \end{aligned} \tag{28}$$

In the general case, a one-dimensional Lagrange element of order will have $p + 1$ nodes and $p + 1$ shape function can be formulated as

$$N_i(s) = \prod_{\substack{j=0 \\ j\neq i}}^{p} \frac{s - s_i}{s_i - s_i}, \qquad i = 0, ..., p \tag{29}$$

4. Performance Application

Some numerical examples to verify the proposed technique. and demonstrate its performance and capabilities. The linear elasticity is considered to demonstrate its capability to treat general boundary conditions. The flexibility of the scaling center also investigates. A high order element is considered with linear element and quadratic elements to discretize both defining curve and the trial and test functions. The accuracy and convergence of numerical solutions are confirmed by benchmarking with available solutions and carrying out via a series of meshes.

4.1. Linear Elastic Plate Under Uniform Load and Prescribed Displacement

The proposed technique is first tested with linear elastic plate. Consider a linear elastic plate ABCD under uniform load and prescribed displacement as shown Fig. 3. The medium is made of a

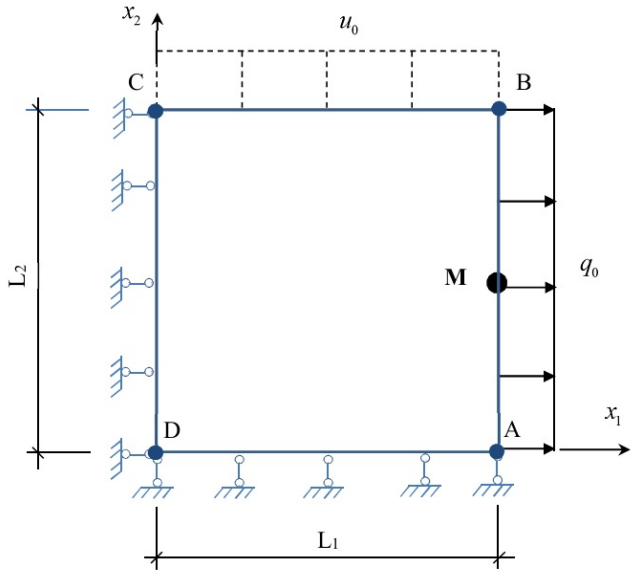

Figure 3. Schematic of a linear elasticity plate under uniform load and prescribed displacement

homogeneous, linearly elastic, isotropic material with Young's modulus E and Poisson's ratio ν, and the modulus matrix $\mathbf{D}$ with non-zero entries $D_{11} = (1-\nu)E/(1+\nu)(1-2\nu)$, $D_{44} = (1-\nu)E/(1+\nu)(1-2\nu)$, $D_{14} = D_{41} = \nu E/(1+\nu)(1-2\nu)$, $D_{23} = E/2(1+\nu)$, $D_{22} = E/2(1+\nu)$, $D_{32} = E/2(1+\nu)$, $D_{33} = E/2(1+\nu)$. The uniform traction q_0 is prescribed on side AD and the uniform displacement u_0 is also described on side BC. To explore the flexibility of scaling center, in the geometry modelling, two different locations of the scaling center, one at center the plate ABCD and the other at the corner D plate are considered and shown in Figs. 4, 5. With the scaling center, the defining curve ABCD is fully prescribed and the other case, defining curve ABC is also described. In the analysis, the Poisson's

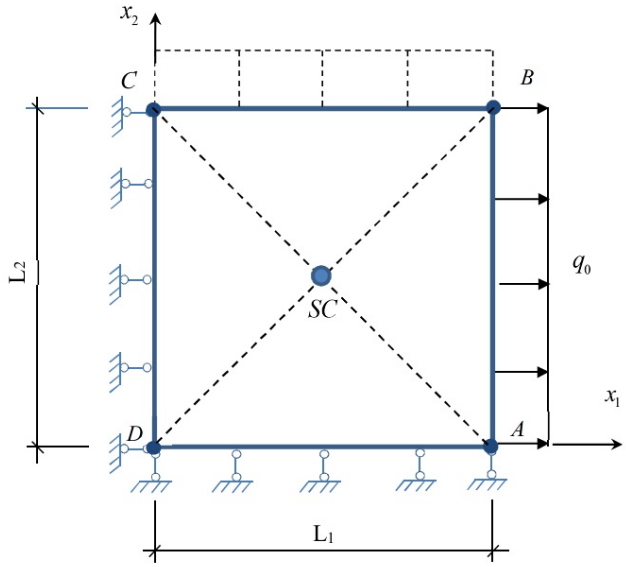

Figure 4. Defining curve corresponding to scaling center at the center of the plate (4 ELM)

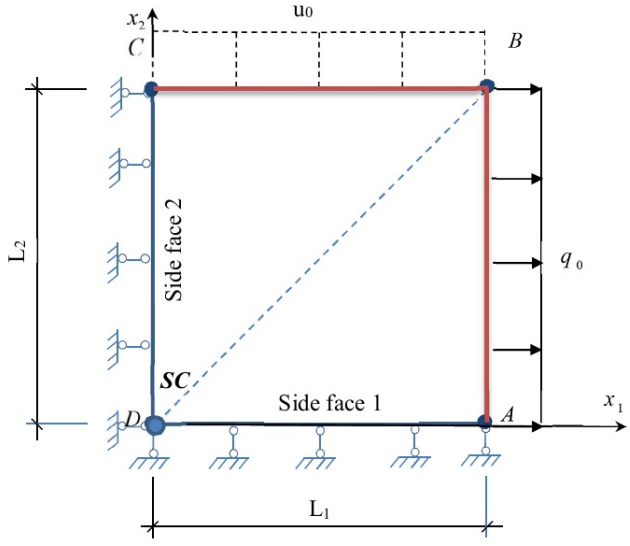

Figure 5. Defining curve corresponding to scaling center at the corner point D (2 ELM)

ratio $\nu = 0.3$ and meshes with N identical linear elements are employed. The results of displacement field and stress field at point M, are reported in Tables 1, 2 for different numbers of meshes. It is seen that the level of accuracy resulting from the two choices of the scaling center is similar. In addition, the numerical solutions converge to the exact solution with only few numbers of element. The present method is also yields highly accurate displacement and stress components.

Table 1. Normalized non-displacement components $u_1/u_0, u_2/u_0$ at point M versus of elements (N) and two locations of scaling center

	AN	Scaling center at the center of plate with meshes N			Scaling center at corner point D with meshes N		
		4	8	16	2	4	8
$\frac{u_1}{u_0}$	0.500000	0.4999995	0.4999995	0.4999996	0.4999995	0.4999995	0.4999996
$\frac{u_2}{u_0}$	1.000000	0.9999948	0.9999962	0.9999975	0.9999962	0.9999962	0.9999975

Table 2. Normalized stress components $\sigma_{11}/q_0, \sigma_{22}/q_0$ at point M versus of elements (N) and two locations of scaling center

	AN	Scaling center at the center of plate with meshes N			Scaling center at corner point D with meshes N		
		4	8	16	2	4	8
$\frac{\sigma_{11}}{q_0}$	1.00000	0.9999986	0.9999994	0.9999997	0.9999986	0.9999994	0.9999997
$\frac{\sigma_{22}}{q_0}$	1.00000	0.9999998	0.9999999	0.9999999	0.9999998	0.9999999	0.9999999

4.2. Linear Elastic Plate Under Mixed Boundary Conditions

As the last example, the linear elastic plate under mixed boundary conditions is chosen to demonstrate the capability of the solving problems with distributed body force and prescribed displacement and traction on the boundary. In addition, the perspective linear and quadratic elements are performed to explore the accuracy of the proposed method. Consider a plane-strain, plate ABCD made of a homogeneous, linearly elastic, isotropic material with Young's modulus E and Poisson's ratio ν as shown in Fig. 6. The matrix $\mathbf{D}$ for this particular problem is the same as the previous example. The constant body force is subjected to the plate $b_1 = (2\nu - 2)\, b_0, b_2 = (2\nu - 2)\, b_0$ with b_0 denoting a constant. The boundary conditions are prescribed on the plate's four sides as follows:

Side AB: $t_1 = b_0\,[(1-\nu)2L_1 + 2\nu x_2]\,; t_2 = 0.$

Side BC: $t_1 = 0; t_2 = b_0\,[2\nu x_1 + 2(1-\nu)L_2].$

Side CD: $u_1 = 0; t_2 = 0.$

Side DA: $t_1 = 0; u_2 = 0.$

From a classical theory of linear elasticity, basing on the plane strain condition, the exact solutions are given by:

- Displacement field:

$$u_1 = \frac{(1+v)(1-2v)}{E} b_0 x_1^1; \quad u_2 = \frac{(1+v)(1-2v)}{E} b_0 x_2^2$$

- Stress field:

$$\sigma_{11} = b_0 \left[(1-v)\, 2x_1 + 2v x_2\right]; \quad \sigma_{22} = b_0 \left[2v x_1 + (1-v) 2x_2\right]; \quad \sigma_{12} = 0$$

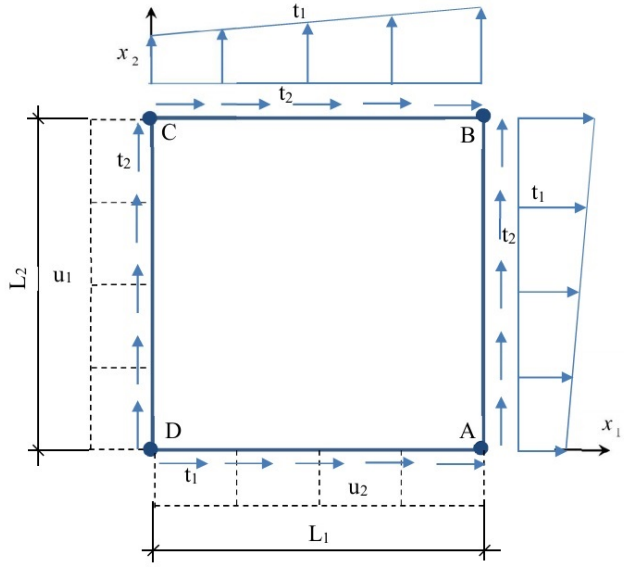

Figure 6. Schematic of a linear elasticity plate under mixed boundary conditions

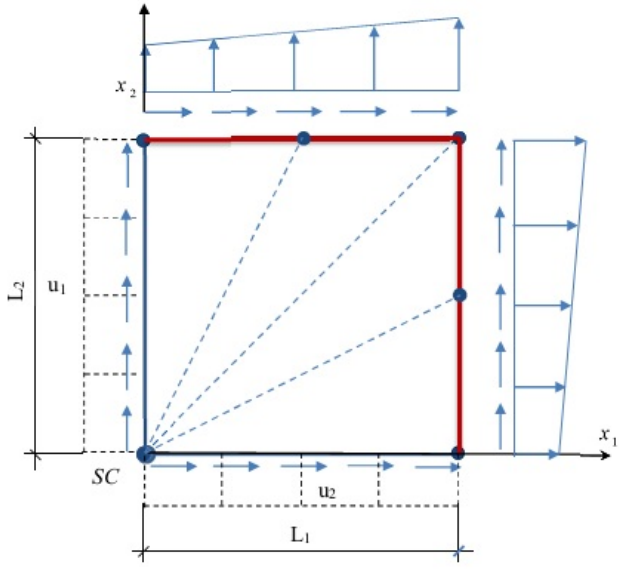

Figure 7. Scaling center and defining cure use in the scaled boundary finite element analysis (4 linear elements case)

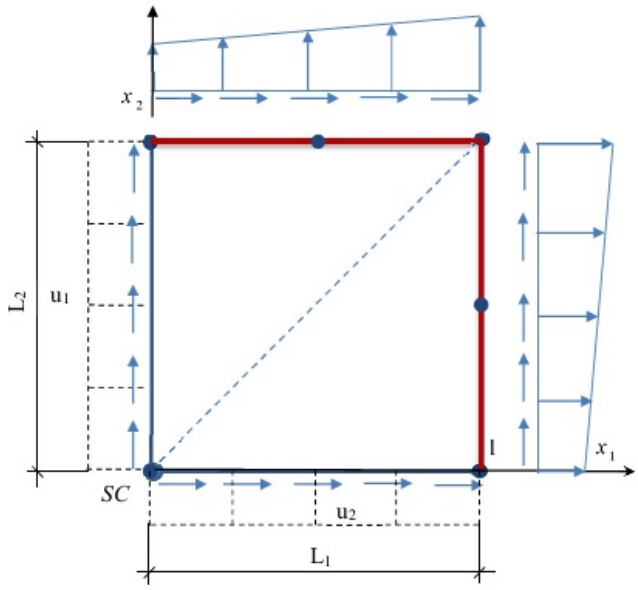

Figure 8. Scaling center and defining cure use in the scaled boundary finite element analysis (2 quadratic elements case)

In the geometry modelling, the scaling center is chosen at the corner of the plate (see Figs. 7, 8). As the result, the boundaries DC and DA become the side faces. In the numerical method, the Poisson's ratio $\nu = 0.3$ and meshes with N identical linear elements and quadratic elements are employed. The normalized non-displacement components and normalized normal stress components at point B are reported in Tables 3, 4. They are seen that use of quadratic elements in the discretization yield higher rate convergence in comparison the linear elements. The normalized displacements $Eu_1/b_0L_1; Eu_2/b_0L_1$ along the line DB are plotted in Fig. 9. It can be seen that the numerical technique convergences to the exact solution as the number of elements N increases and only few elements is sufficient to obtain accurate displacement. The normalized normal stress $\sigma_{11}/b_0L_1, \sigma_{22}/b_0L_1$ along the diagonal line DB are also reported in Figs. 10. Similar to the displacements, the stress components are also obtained in the good behavior. It can be seen that the quadratic elements have clearly yield higher rate convergence. This implies that converged resulting for specified tolerance can be obtained with few quadratic elements.

Table 3. Normalized non-displacement components $u_1/u_1^{AN}, u_2/u_1^{AN}$ at point B versus number of elements (N) for both linear and quadratic elements

	AN	SBFEM versus number of linear elements (N)			SBFEM versus number of quadratic elements (N)		
		4	8	16	2	4	8
$\frac{u_1}{u_1^{AN}}$	1.000000	0.985042	0.996970	0.999464	1.000000	1.000000	1.000000
$\frac{u_2}{u_1^{AN}}$	1.000000	0.985042	0.996970	0.999464	1.000000	1.000000	1.000000

Table 4. Normalized normal stress components $\sigma_{11}/\sigma_{11}^{AN}, \sigma_{22}/\sigma_{22}^{AN}$ at point B versus of elements (N) for both linear and quadratic Elements

	AN	SBFEM versus number of linear elements (N)			SBFEM versus number of quadratic elements (N)		
		4	8	16	2	4	8
$\frac{\sigma_{11}}{\sigma_{11}^{AN}}$	1.000000	0.932285	0.967448	0.983845	1.000000	1.000000	1.000000
$\frac{\sigma_{22}}{\sigma_{11}^{AN}}$	1.000000	0.832080	0.917423	0.959023	1.000000	1.000000	1.000000

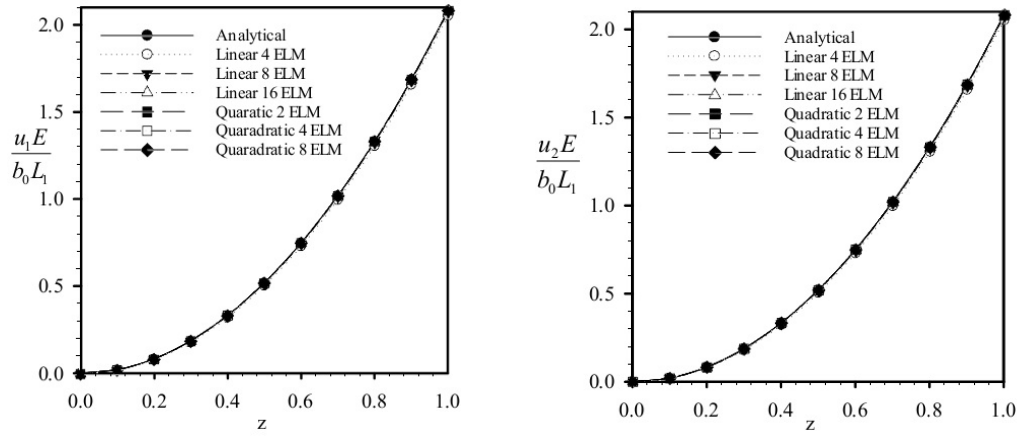

(a) $u_1 E/b_0 L_1$ (b) $u_2 E/b_0 L_1$

Figure 9. Normalized non-displacement components along the diagonal line DB of the elasticity plate under mixed boundary conditions

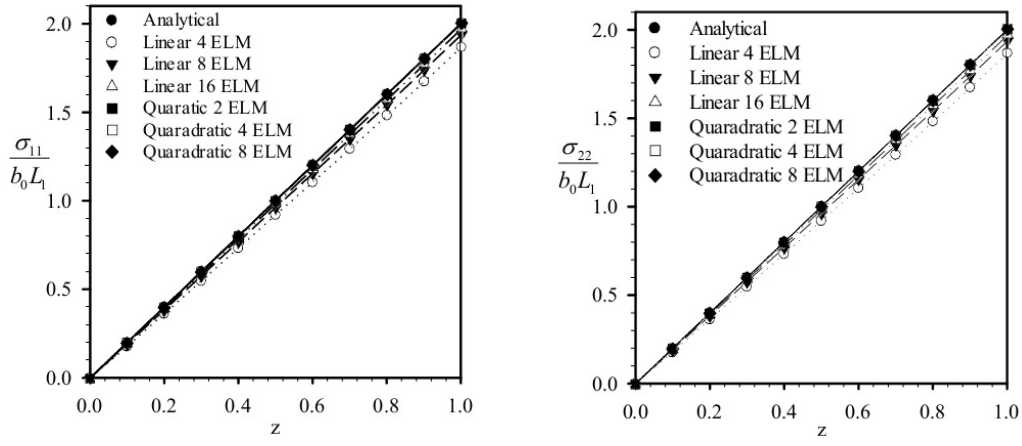

(a) $\sigma_{11}/b_0 L_1$ (b) $\sigma_{22}/b_0 L_1$

Figure 10. Normalized normal stress components along the diagonal line DB of the elasticity plate under mixed boundary conditions

5. Conclusions

The scaled boundary finite element equations have been successfully developed for analysis two-dimensional linear problem. The formulation has been established to use high-order polynomial element to form the approximation in the circumferential direction. It is also established in a general framework for treating mixed boundary conditions, the prescribed body force and contribution of the side face. In addition, the position of the scaling center is explored the accuracy of prosed method. Results from some numerical study have indicated that the resulting is similar for both the positions of the scaling center. The quadratic elements show higher rate of convergence in comparison with the linear elements.

Acknowledgments

This work belongs to the project in 2021 funded by Ho Chi Minh City University of Technology and Education, Vietnam.

References

[1] Wolf, J. P. (2003). *The scaled boundary finite element method*. John Wiley & Sons.
[2] Wolf, J. P., Song, C. (1996). *Finite-element modelling of unbounded media*. Wiley Chichester.
[3] Vu, T. H., Deeks, A. J. (2006). Use of higher-order shape functions in the scaled boundary finite element method. *International Journal for Numerical Methods in Engineering*, 65(10):1714–1733.
[4] He, Y., Yang, H., Xu, M., Deeks, A. J. (2013). A scaled boundary finite element method for cyclically symmetric two-dimensional elastic analysis. *Computers & Structures*, 120:1–8.
[5] Zou, D., Teng, X., Chen, K., Yu, X. (2018). An extended polygon scaled boundary finite element method for the nonlinear dynamic analysis of saturated soil. *Engineering Analysis with Boundary Elements*, 91: 150–161.
[6] Wallner, M., Birk, C., Gravenkamp, H. (2020). A scaled boundary finite element approach for shell analysis. *Computer Methods in Applied Mechanics and Engineering*, 361:112807.
[7] Li, C., Man, H., Song, C., Gao, W. (2013). Fracture analysis of piezoelectric materials using the scaled boundary finite element method. *Engineering Fracture Mechanics*, 97:52–71.
[8] Liu, J., Lin, G. (2012). A scaled boundary finite element method applied to electrostatic problems. *Engineering Analysis with Boundary Elements*, 36(12):1721–1732.
[9] Vu, T. H., Deeks, A. J. (2013). Using fundamental solutions in the scaled boundary finite element method to solve problems with concentrated loads. *Computational Mechanics*, 53(4):641–657.
[10] Chung, N. V. (2019). Scaled boundary finite element method with circular defining curve for geo-mechanics applications. *Journal of Science and Technology in Civil Engineering (STCE) - NUCE*, 13 (3):124–134.
[11] Ooi, E. T., Song, C., Tin-Loi, F., Yang, Z. J. (2012). Automatic modelling of cohesive crack propagation in concrete using polygon scaled boundary finite elements. *Engineering Fracture Mechanics*, 93:13–33.
[12] Wang, X., Jin, F., Prempramote, S., Song, C. (2011). Time-domain analysis of gravity dam–reservoir interaction using high-order doubly asymptotic open boundary. *Computers & Structures*, 89(7-8):668–680.
[13] Gravenkamp, H., Song, C., Prager, J. (2012). A numerical approach for the computation of dispersion relations for plate structures using the Scaled Boundary Finite Element Method. *Journal of Sound and Vibration*, 331(11):2543–2557.
[14] Man, H., Song, C., Gao, W., Tin-Loi, F. (2012). A unified 3D-based technique for plate bending analysis using scaled boundary finite element method. *International Journal for Numerical Methods in Engineering*, 91(5):491–515.

[15] Man, H., Song, C., Xiang, T., Gao, W., Tin-Loi, F. (2013). High-order plate bending analysis based on the scaled boundary finite element method. *International Journal for Numerical Methods in Engineering*, 95 (4):331–360.

[16] Man, H., Song, C., Gao, W., Tin-Loi, F. (2014). Semi-analytical analysis for piezoelectric plate using the scaled boundary finite-element method. *Computers & Structures*, 137:47–62.

[17] Gravenkamp, H., Birk, C., Song, C. (2015). Simulation of elastic guided waves interacting with defects in arbitrarily long structures using the Scaled Boundary Finite Element Method. *Journal of Computational Physics*, 295:438–455.

[18] Chen, X., Birk, C., Song, C. (2015). Transient analysis of wave propagation in layered soil by using the scaled boundary finite element method. *Computers and Geotechnics*, 63:1–12.

[19] Gravenkamp, H. (2018). Efficient simulation of elastic guided waves interacting with notches, adhesive joints, delaminations and inclined edges in plate structures. *Ultrasonics*, 82:101–113.

[20] Zhang, J., Eisenträger, J., Duczek, S., Song, C. (2020). Discrete modeling of fiber reinforced composites using the scaled boundary finite element method. *Composite Structures*, 235:111744.